Polar Meteorol. Glaciol., **18**, 54–71, 2004

Greenland Ice Sheet and rising sea level in a worst-case climate change scenario

Terry Hughes

Department of Earth Sciences, Climate Change Institute, Bryand Global Science Center, University of Maine, Orono, Maine 04469, U.S.A.
E-mail: terry.hughes@maine.edu

(Received September 25, 2003; Accepted July 31, 2004)

Abstract: Models that simulate sheet flow in the Greenland Ice Sheet balance forces at gridpoints in the map plan, which allows only a slow response to changes in climate forcing. A holistic approach to modeling allows a rapid response that takes place in ice streams. Holistic modeling results are presented that lengthen and lower the profiles of Greenland ice streams. This occurs because surface meltwater from "greenhouse" warming reaches the bed through crevasses, and thereby increases basal water pressure. Thinning is then controlled primarily by increased basal water pressure that lengthens ice streams. If thinning caused by this process is both rapid and simultaneous for the major Greenland ice streams, the resulting iceberg outbursts might trigger an episode of rapid climate change.

key words: Greenland Ice Sheet, sea level, climate change, ice streams, icebergs

1. Introduction

In a worst-case scenario, abrupt climate change occurs when partial gravitational collapse of the Greenland Ice Sheet is great enough and fast enough to halt production of North Atlantic Deep Water (NADW). Shutdown of NADW during Quaternary glaciations was first noted by Schnitker (1979). Broecker and Denton (1989) globalized this shutdown by postulating a worldwide oceanic "conveyor belt" that caused a cold "mode flip" in climate when a halt in NADW production stopped the conveyor-belt current.

According to Broecker and Denton (1989), warm water in the North Atlantic Current (NAC) delivers 10.5×10^8 J m^{-2} a^{-1} to the sites of NADW production north of Iceland and in the Labrador Sea. Suppose the Greenland Ice Sheet releases 8×10^5 km^3 of icebergs that drift into these sites. If the icebergs average -20°C, then 8.35×10^4 J kg^{-1} of sensible heat and 3.34×10^5 J kg^{-1} of latent heat are needed to melt them. They provide 30.6×10^{22} J to cool 10^6 km^2 of ocean area where NADW is produced. The NAC heat input over this area is 10.5×10^{20} J a^{-1}. Therefore NADW production might be suppressed for up to 300 years, the time needed for the NAC heat flux to melt Greenland icebergs. It is noteworthy that the draft of these tabular icebergs, up to 500 m, is comparable to the 800 m depth of the NAC. This could trigger an abrupt cold

shift in climate in lands surrounding the North Atlantic that lasts 300 years (Hughes, 1998, p. 10–11). A cold shift in Greenland spanned from the end of the Norse settlements in 1379 to resettlement in 1721, a period of 342 years (Erngaard, 1972). Similar shifts in climate have been documented repeatedly over the past 110000 years from the GISP 2 Greenland ice core by Mayewski *et al*. (1997). In the worst-case scenario examined here, 300 years will be taken as the timeframe for partial gravitational collapse of the Greenland Ice Sheet. Whether this ice lowering can be linked to "greenhouse" warming that triggers a cold period lasting 300 years will depend on how much lowering takes place.

A longstanding and still unresolved dispute in glaciology is whether gravitational forcing in ice sheets should be balanced locally at gridpoints in the map-plane, or holistically along the whole length of ice flowlines. The most advanced models simulate three-dimensional time-dependent flow in the map plane, using a shallow-ice approximation (Hutter, 1983) to treat heat and mass flow in the vertical dimension (*e.g*., Greve, 1997). The first comprehensive applications of this approach to the Greenland Ice Sheet that took account of past, present, and future climate changes, including "greenhouse" warming, were by Huybrechts *et al*. (1991), Letréguilly *et al*. (1991), and Huybrechts (1994, 1996), using an ice-sheet model originally developed and applied to simulate evolution of the Antarctic Ice Sheet (Huybrechts, 1990). These are essentially climate-driven models in which ice temperature and mass balance changes over time at the ice surface, after lag times controlled by ice flow, eventually produce changes in the basal thermal regime, notably basal ice temperatures where the bed is frozen and basal melting or freezing rates where the bed is thawed. Such calculations require specifying a poorly constrained geothermal heat flux at the bed. With careful tuning of parameters, however, these models give excellent simulations of the present-day behavior of the ice sheets covering Greenland and Antarctica. Their major weakness is that, by tying gravitational forcing to the local basal shear stress at model gridpoints, these models are unable to simulate the dynamics of ice streams, which are fast currents of ice that drain 50% of the Greenland Ice Sheet and 90% of the Antarctic Ice Sheet. Jakobshavn Isbrae, shown in Fig. 1, is the fastest and most studied Greenland ice stream. Its current rapid dynamic thinning guides this study.

Over the next few centuries, according to the modeling experiments by Huybrechts *et al*. (1991) and Huybrechts (1994, 1996), changes in the size and shape of the Greenland Ice Sheet will consist in general of interior ice thickening due to increased snow accumulation accompanied by steepening and retreat of ice margins due to increased summer ice melting. The major ice streams in Fig. 1 are not producing this behavior. As first reported for Kangerdlugssuaq Gletscher on the east coast (Thomas *et al*., 2000) and now for Jakobshavn Isbrae on the west coast (Thomas, 2004), ice thinning is propagating inland up these ice streams, and is accompanied by increased ice discharge rates that tend to keep the grounded ice margin relatively stable or perhaps even advancing due to forward advection of thick interior ice. In this case, instead of interior thickening and retreating margins, there will be interior thinning and stable or advancing margins. Such opposite behavior is manifested only in ice streams, but they discharge half of Greenland ice and control NADW production by releasing large icebergs.

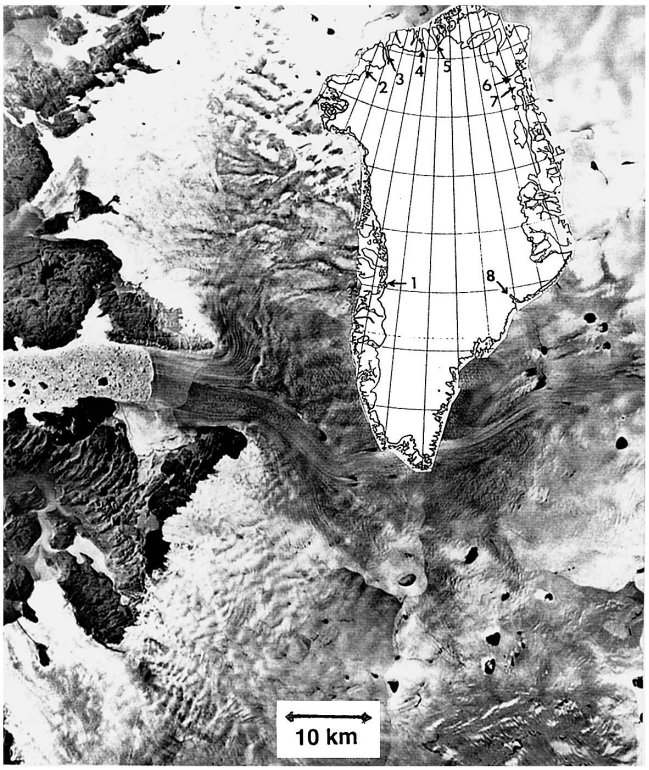

Fig. 1. Jakobshavn Isbrae and other thinning ice streams in Greenland. Jakobshavn Isbrae is depicted in a photomosaic by H.H. Brecher (Hughes, 1998, Figure 1.4). Ice streams and their ice drainage basins that are known to be thinning at present are (1) Jakobshavn Isbrae, (2) Humboldt Gletscher, (3) Petermann Gletscher, (4) Ryder Gletscher, (5) Ostenfeld Gletscher, (6) Nioghalvjferdsbrae Gletscher, (7) Zacherias Isstrom, and (8) Kangerdlugssuaq Gletscher (Joughin et al., 1996a, b; Rignot et al., 1997; Thomas et al., 2000, 2003; W. Krabill, personal communication, 2001).

Modeling ice streams probably requires a holistic approach, since present-day ice streams in Greenland, and especially in Antarctica, are transitional between sheet flow of the kind modeled by Huybrechts (1990), Huybrechts *et al*. (1991), Letréguilly *et al*. (1991), and Huybrechts (1994, 1996), and shelf flow of the kind originally modeled in Antarctica by MacAyeal and Thomas (1982) for the Ross Ice Shelf and by Lange and MacAyeal (1986) for the Filchner-Ronne Ice Shelf. Weis *et al*. (1999) present a state-of-the-art ice-shelf model. For sheet flow, gravitational forcing is linked to the product of ice thickness and ice surface slope, and is adequately balanced by the basal drag force (Orowan, 1949; Nye, 1952). When ice sheets become afloat in deep water and form ice shelves, gravitational forcing for shelf flow is linked to ice height floating above water and is balanced by longitudinal tension (Weertman, 1957a) and, in fjords or embayments, by side drag and local grounding (Thomas, 1973a, b). Ice streams that begin as converging sheet flow and end as free or confined shelf flow should probably be modeled as stream flow in which gravitational forcing linked to ice thickness, slope, and

height floating above water is balanced by resisting forces that are dominated by basal drag at the beginning of stream flow, but then become increasingly dominated by side drag and longitudinal forces along the ice stream, with longitudinal tension being reduced by water buttressing and by ice-shelf buttressing if shelf flow is hampered by sidewalls and basal pinning points. These changes in forcing and resistance along an ice stream are best treated using a holistic approach to ice-sheet modeling.

2. Holistic modeling

A holistic approach assumes that gravitational forces at some distance x upslope along an ice-sheet flowband must be balanced not only by local resisting forces, but also by all downslope forces that resist flow, beginning at the ice-sheet margin. This includes a back-force from water pressure when the ice margin is grounded or floating in water, and basal and side shear forces under and alongside the flowband summed over distance x. The holistic approach employed in this study allows gravitational forcing caused by the height at x of ice above land or water at the ice margin ($x=0$) to be transmitted upslope along a flowband on a thawed bed, with basal buoyancy being the vehicle for transmission. An ice sheet generally creeps by longitudinal extension in the accumulation zone and by longitudinal compression in the ablation zone, except along ice streams, as it responds to the mass balance. In the mass balance used here, ice has thickness h_I at distance x from the origin of axes x, y, z, with x and y in horizontal directions, x positive upslope, y positive along ice elevation contours, and z positive upward in the vertical direction. In this treatment, x is positive toward the center of ice spreading, and follows ice flowbands having variable width w_I. The mass balance is computed for constant ice accumulation rate a, ice thickness h_I that depends on bed topography and the degree of ice-bed coupling, and ice velocity u_x (negative u_x because ice flows in the minus x direction).

The holistic flowband model used here employs a geometrical force balance in which longitudinal deviatoric tensile stress σ_T for an ice stream of constant width is (Hughes, 2003):

$$\sigma_T = 1/2\rho_I h g_I [1-(\rho_I/\rho_W)] [P_W/P_I]^2, \quad (1)$$

where ρ_I is ice density, ρ_W is water density, g is gravity acceleration, h_I is ice thickness, $P_W=\rho_W g h_W$ is basal water pressure that supports water height h_W, and $P_I=\rho_I g h_I$ is ice overburden pressure. The degree of ice-bed coupling is related to $P_W/P_I=\rho_W h_W/\rho_I h_I$ in eq. (1) through a compressive force F_C that is cumulative along distance x from the ice front, where $x=0$, $F_C=(F_C)_O$, and $P_W/P_I=(P_W/P_I)_O$. If the ice front is on dry land, $(F_C)_O=0$ because $(P_W/P_I)_O=0$. If the ice front is in water, $(F_C)_O>0$ because $0<(P_W/P_I)_O\leq 1$. Ratio P_W/P_I in eq. (1) is a basal buoyancy factor at x such that $P_W/P_I=0$ for a frozen bed, $P_W/P_I=1$ when all the ice overburden is supported by basal water for a thawed bed, and $0<P_W/P_I<1$ when part of the ice overburden is supported by basal water and part by the bed.

For Greenland ice streams, a longitudinal deviator compressive stress σ_C arises from average water pressure P_W at the ice-shelf calving front, its increase to the ice-shelf grounding line, and from both side shear stress τ_S and basal shear stress τ_O averaged over

distance x from the calving front, where τ_O exists in an ice shelf of floating length L at basal pinning points that produce ice rumples on the top surface (Thomas, 1973a, b). Compressive force F_C has several components that contribute to P_W/P_I and σ_C at x:

$$\begin{aligned} F_C &= (1/2\rho_I g h_I) w_I h_I - \sigma_T w_I h_I = \sigma_C w_I h_I = \sigma_C A_x \\ &= (\overline{P}_W A_W)_O + \int_O^L [\,\partial(\overline{P}_W A_W)/\partial x\,]\,\mathrm{d}x + \overline{\tau}_S A_y + \overline{\tau}_O A_z \\ &= (1/2\rho_W g h_W)_O (w_I h_W)_O + \int_O^L [\,\partial(1/2\rho_W g w_I h^2_W)/\partial x\,]\,\mathrm{d}x + 2\overline{\tau}_S \overline{h}_I x + \overline{\tau}_O \overline{w}_I x, \end{aligned} \quad (2)$$

where $A_x = \mathrm{w_I h_I}$ is the transverse cross-sectional area of ice at distance x upslope from the ice-shelf calving front, $A_W = w_I h_W$ is the transverse cross-sectional area of water that buttresses an ice flowband of width w_I, $A_y = 2\overline{h}_I x$ is the side area of ice for average ice thickness $\overline{h}_I$ from x to the calving front, and $A_z = \overline{w}_I x$ is the basal area of ice for average flowband width $\overline{w}_I$ along x. Hydrostatic force $(\overline{P}_W A_W)_O$ and hydrostatic force gradient $\partial(\overline{P}_W A_W)/\partial x$ are determined at the calving front ($x = 0$) and along length L of the ice shelf, respectively. Solving for σ_C:

$$\begin{aligned} \sigma_c &= \frac{\rho_I g h_I}{2} - \frac{\rho_I g h_I}{2}\left(1 - \frac{\rho_I}{\rho_W}\right)\left(\frac{P_W}{P_I}\right)^2 = \frac{(\rho_W g w_I h^2_W)_O}{2 w_I h_I} \\ &+ \frac{\int_O^L [\partial(\rho_W g w_I h^2_W)/\partial x]\,\mathrm{d}x}{2 w_I h_I} + \frac{2\overline{\tau}_S \overline{h}_I x}{w_I h_I} + \frac{\overline{\tau}_O \overline{w}_I x}{w_I h_I}. \end{aligned} \quad (3)$$

Therefore, P_W/P_I at x depends on downslope water buttressing of floating ice and ice-bed coupling of grounded ice.

Basal shear stress τ_O, averaged along grounded length $x - L$ in eq. (3), can be linked to P_W/P_I using the approach described by Hughes (1998, p.105–106). In this approach:

$$\begin{aligned} \tau_O &= \rho_I g\,[h_I - (\rho_W/\rho_I) h_W]\,\Delta h/\Delta x = \rho_I g h_I (1 - P_W/P_I)\,\Delta h/\Delta x \\ &= B(1 - P_W/P_I)^{2c} u_s^{1/m} = C(P_I - P_W)^s u_s^{1/m}, \end{aligned} \quad (4)$$

where $h_I(1 - P_W/P_I)$ is the part of h_I that is supported by the bed, not by basal water, B is a basal sliding parameter, and u_s is the basal sliding velocity, which closely approaches the ice surface velocity as P_W/P_I increases. Equation (4) reduces to the Weertman (1957b) theoretical sliding velocity when $P_W/P_I \approx 0$, $c = 1$, and $m = 2$. It coincides with the Budd *et al*. (1979) experimental sliding velocity when $C = B/P_I^s$, $s = 2c \approx 1/3$, and $m \approx 3$.

Ice thinning over time causes the bed to isostatically rebound, which changes the surface slope from $\Delta h/\Delta x$ to $\Delta h^*/\Delta x$ and ice thickness from h_I to $h_I{}^*$. If no rebound occurs at the grounding line, then ice elevation h is related to rebounding elevation h^* by $h = h_G + (1 + r)^{1/2}(h^* - h_G)$, where r is an isostasy ratio and h_G is water depth at the grounding line (Hughes, 1998, p. 61). Making this substitution and combining the force balance with the mass balance for a flowband of constant width and variable ice thinning rate $\delta h_I/\delta t$, for ice thickness h_O and ice velocity u_O at $x = 0$, and using $h_R = h - h_I$ for present-day bedrock elevation above or depth below sea level, with A and n being the respective ice hardness parameter and viscoplastic parameter in the flow law of ice

$\dot{\varepsilon}_{xx}=(\sigma_T/A)^n$ for longitudinal strain rate $\dot{\varepsilon}_{xx}$, the surface slope for an isostatically rebounding thinning ice sheet is as derived by Hughes (1998, p. 54–56), except that side shear stress τ_S is multiplied by P_W/P_I so that side drag decreases as basal drag increases upslope along an ice stream of width w_I to give τ_O in eq. (4). Then the ice-surface slope on an isostatically rebounding bed is:

$$\frac{\Delta h^*}{\Delta x}=\frac{(1-\rho_I/\rho_W)}{(1+r)^{1/2}}\left(\frac{P_W}{P_I}\right)^2\left\{\frac{[a-\delta h_I/\delta t]\,[h_G+(1+r)^{1/2}(h^*-h_G)-h_R]}{(a-\delta h_I/\delta t)x+h_0u_0}\right.$$
$$\left.-\frac{[h_G+(1+r)^{1/2}(h^*-h_G)-h_R]^{n+2}}{(a-\delta h_I/\delta t)x+h_0u_0}\left[\frac{\rho_I g_z}{4A}\left(1-\frac{\rho_I}{\rho_W}\right)\left(\frac{P_W}{P_I}\right)^2\right]^n\right\}$$
$$+\frac{[h_G+(1+r)^{1/2}(h^*-h_G)-h_R]}{2(1+r)^{1/2}}\left(1-\frac{\rho_I}{\rho_W}\right)\frac{\Delta}{\Delta x}\left(\frac{P_W}{P_I}\right)^2+\frac{2\tau_S(P_W/P_I)}{(1+r)^{1/2}\rho_I g_z w}$$
$$+\frac{\tau_O}{(1+r)^{1/2}\rho_I g_z[h_G+(1+r)^{1/2}(h^*-h_G)-h_R]}. \qquad (5)$$

Both σ_T given by eq. (1) and its gradient $\Delta\sigma_T/\Delta x$ are incorporated into eq. (5) through P_W/P_I and its gradient $\Delta(P_W/P_I)/\Delta x$. Equation (5) reduces to pure sheet flow (Nye, 1952) as $P_W/P_I\to 0$ and to pure shelf flow (Van der Veen, 1983) as $P_W/P_I\to 1$, taking $\tau_S=r=0$ for both cases. Assuming present-day glacial isostatic equilibrium, for which $r=0$ at time $t=0$, then future basal rebound at time t due to ice thinning is given by $r=r_o\,[\exp(-t/t_o)-1]$ for a time constant of $t_o=5000\,a$ (Andrews, 1970) and $r_o=\rho_I/(\rho_R-\rho_I)$ for density ρ_R of mantle rock.

Note that $\tau_O=0$ when $P_W/P_I=1$ in eqs. (4) and (5). This is the condition for shelf flow. Therefore eq. (4) applies only for $0\le P_W/P_I<1$ and allows τ_O in eq. (5) to be expressed in terms of P_W/P_I, which then becomes the critical variable in modeling transitions from sheet flow to stream flow to shelf flow. The observation for some Antarctic ice streams is that P_W increases upslope, so that subglacial meltwater flows down the hydraulic gradient and is discharged across the grounding line (*e.g.*, Engelhardt and Kamb, 1997; Tulaczyk *et al*., 2001a). However, h_W must eventually decrease to zero if the bed is frozen at the ice divide, which is the case in Greenland. When h_W is sufficiently small, sheet flow replaces stream flow. Equation (4) requires that bedrock bumps become progressively drowned by basal water or buried by water-saturated basal till that provides little resistance to motion of the overlying ice. Tulaczyk *et al*. (2001b) have analyzed basal sliding when till is composed of Tertiary sediments having a low yield stress so that u_s is independent of τ_O. If the Greenland Ice Sheet lies on a Precambrian crystalline shield, eq. (4) may be more appropriate for sliding. Since P_W rises with h_W, $P_W/P_I=0$ for a frozen bed and $P_W/P_I\approx 0$ for a thawed bed in regions where the ice load is supported by the bed because only a thin film of basal water is present (Weertman, 1957b). This is the condition for sheet flow, except where subglacial lakes require that $P_W/P_I=1$.

For sheet flow, in which it is assumed that P_W/P_I is zero (frozen bed) or small (thawed bed), because $0\le h_W\ll 1$, it is also assumed that the fraction f_T of the bed that is thawed changes from $f_T=0$ along ice divides to $f_T=1$ at the heads of ice streams such

that, if $(\tau_O)_s$ and $(\tau_O)_c$ are the respective basal shear stresses for sliding on a thawed bed and creep over a frozen bed (Wilch and Hughes, 2000):

$$\tau_O = f_T(\tau_O)_s + (1 - f_T)(\tau_O)_c. \tag{6}$$

Theoretical expressions relating $(\tau_O)_s$ and $(\tau_O)_c$ to the mass balance are derived in Hughes (1998, p. 153–165) for both variable and constant accumulation rates over an ice sheet.

For stream flow the assumption is that P_W/P_I increases from the heads of ice streams to their grounding lines, where they may become afloat, as does Jakobshavn Isbrae. Therefore $f_T = 1$. Although variations in basal conditions, notably subglacial hydrology linked to bedrock topography, would cause an irregular increase of P_W/P_I, lack of knowledge of subglacial hydrology allows consideration of a regular increase. One function that gives a regular increase is $P_W/P_I = (1 - x/L_s)^c$, where x is distance along an ice sheet flowline when $x = 0$ at the ice-shelf grounding line and $x = L_s$ at the ice divide. Selecting a value of c between zero and infinity produces a first-order fit to the profile of any ice stream (Hughes, 1998, Figures 6.8–6.10). Another function for which P_W/P_I and $\partial(P_W/P_I)/\partial x$ are both continuous produces a slightly better first-order fit to the profiles of present-day Greenland ice streams:

$$\frac{P_W}{P_I} = \cos^c\left(\frac{\pi x}{2L_s}\right). \tag{7}$$

In eq. (7), $0 < c < \infty$, with $c = 0$ for pure shelf flow and $c = \infty$ for pure sheet flow (Hughes, 1998, p. 81–83). Stream flow can progressively convert sheet flow to shelf flow in time $t = t_c$ if, for example, $c = (t_c - t)/t$. Using eq. (7) for P_W/P_I in eq. (5) eliminates the need for calculating P_W/P_I from eq. (3), which is physically based but requires knowing how $\partial(\rho_W g w_I h_W^2)/\partial x$, τ_S, τ_O, h_I, and w_I vary along x. This would require a precise knowledge of how and how much surface meltwalter reaches the bed along x, and of subglacial hydrology along x.

3. Application and results

Recent studies by Zwally *et al*. (2002) just north of Jakobshavn Isbrae (Fig. 1) have linked increased surface velocity with increased surface melting, as measured by an increase in positive-degree-day totals. They concluded that some surface meltwater was reaching the bed by way of crevasses and moulins, thereby increasing basal sliding velocities. Their conclusion has been reinforced strongly by the current dramatic acceleration and thinning of Jakobshavn Isbrae itself, with ice thinning propagating some 100 km or more into the Greenland Ice Sheet (Thomas *et al*., 2003; Thomas, 2004). I use the holistic model to calculate whether ice thinning over 300 years of ongoing "greenhouse" warming will discharge enough icebergs from major ice streams to shut down NADW production, and thereby trigger an episode of abrupt climate cooling.

My holistic approach to ice-sheet modeling produces stream flow that includes both the longitudinal gravitational force generated by ice thickness and surface slope, which

drives sheet flow, and the longitudinal gravitational force generated by ice thickness supported by basal water pressure, which drives shelf flow (Hughes, 1992). This recognizes that stream flow is transitional between sheet flow and shelf flow. Figure 2 is a cartoon showing how basal buoyancy, represented by the height h_W that basal water would rise in a borehole due to basal water pressure P_W, can lower the surface profile of an ice sheet as basal buoyancy propagates up ice streams when surface meltwater reaches the bed through crevasses and moulins during climate warming. If basal buoyancy is minor, and located only in the vicinity of an ice-self grounding line, the concave profile of stream flow quickly becomes the convex profile of sheet flow. A rise of the snowline due to climate warming will then allow the equilibrium line to retreat only a relatively short distance up the steep convex ice slope, shown as the short thick line segments in Fig. 2. This is all that is allowed in the model used by Letréguilly *et al*. (1991) and by Huybrechts (1994, 1996). However, if surface meltwater passes through crevasses and moulins to the bed, as inferred by Zwally *et al*. (2002) from their correlation of surface melting rates and ice velocity just north of Jakobshavn Isbrae, basal buoyancy becomes major and extends throughout the ablation zone, thereby greatly extending the concave profile of stream flow. Then the same rise in the snowline causes the equilibrium line to retreat a much longer distance up the gentle concave ice slope, shown as the long thick line segment in Fig. 2. The resulting loss in ice elevation and volume along the flowline, after a new profile has been calculated, is considerably greater than if basal buoyancy had remained localized near the grounding line. Ice surface lowering caused by enhanced basal buoyancy in this study employs the same dependence of surface melting rates on ice elevation that was used by Letréguilly *et al*. (1991) and by Huybrechts (1994). Surface meltwater is assumed to reach the bed throughout the ablation zone.

Equation (5) is solved numerically to generate flowline profiles that lower pro-

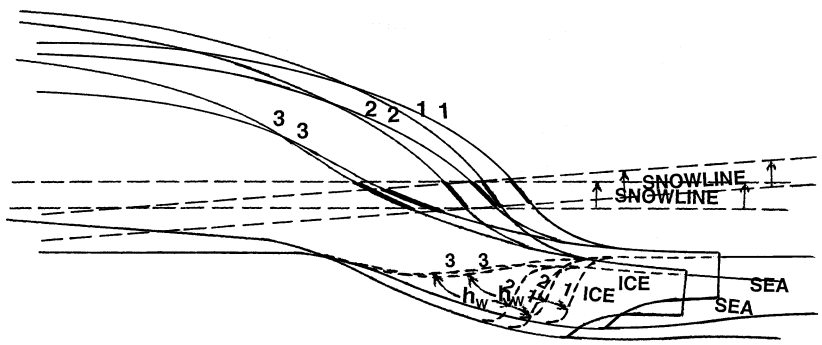

Fig. 2. A cartoon showing how increasing basal buoyancy lowers the surface profile of the Greenland Ice Sheet. Basal buoyancy increases inland when a rise in the snowline widens the ablation zone inland and crevasses transport some surface meltwater to the bed. Profile 1 represents the present ice surface. Profiles 2 and 3 represent future ice surfaces when basal buoyancy, represented by h_W, is localized near the grounding line and extends across the ablation zone, respectively, giving respective convex and concave surface profiles. The bold segments of the three profiles show that the same snowline rise widens the ablation zone much more when increasing basal buoyancy makes a convex profile concave.

gressively as surface meltwater reaches the bed, increasing P_W/P_I and causing c in eq. (7) to decrease with time t along grounded length L_S of an ice sheet flowline. Let function $\phi(h^*)$ represent everything to the right of the equals sign in eq. (5). Then $\Delta h^*/\Delta x = \phi(h^*)$. The numerical solution for h^* employs Euler's method. Each ice flowline is divided into i steps, each of length $\Delta x = 20$ km, with $i = 0$ at the grounded ice margin. Then $\Delta h^* = h^*_{i+1} - h^*_i$ at any given Δx step and eq. (5) can be written as an initial-value finite-difference recursive formula:

$$h^*_{i+1} = h^*_i + \phi(h^*_i)\Delta x. \tag{8}$$

The initial value ($i = 0$) must be specified at the grounded ice margin for each flowline, and Δx is the finite difference. Most ice margins are grounded in water of known or assumed depth h_G, where $h^*_{i=0} = h_{i=0}$ because no isostatic change is allowed. Then the first Δx step begins at $h^*_0 = h_0 = h_G(1 - \rho_I/\rho_W)$, assuming the grounding line is at the flotation depth for ice. Some ice flowlines end on dry land, notably in southwest Greenland. In these cases, a parabolic flowline profile is assumed for a short distance x, so the first Δx step begins at $h^*_0 = h_0 = h_R + (2\tau_O x/\rho_I g)^{1/2}$ for $x = 1$ km and $\tau_O = 100$ kPa is the yield stress of ice. Equation (8) produces a flowline profile steeper than the analytical parabolic profile (Nyhoff and Leestma, 1996, p. 353), a defect not important when comparing present and future ice elevations, as in this study. Using eq. (8) to solve eq. (5) for the present and the future was done by setting $\delta h^*_I/\delta t = 0$ in eq. (5) for both times, then using the ice thickness change to calculate $\delta h^*_I/\delta t$ over that time, and then solving eq. (5) again for the future time. Raymond *et al.* (2001) report $\tau_S = 150$ kPa is typical for West Antarctic ice streams. This value of τ_S is reasonable in applying eq. (5) to Greenland ice streams. Assuming basal sliding dominates stream flow, the mass-balance velocity for stream flow is taken to be u_s in eq. (4), which is then used to replace τ_O in eq. (5).

Figure 3 shows calculated ice-elevation contours at 200 m intervals that match present-day ice-elevation contours of the Greenland Ice Sheet within 50 m, as seen by comparison with a map also contoured at 200 m intervals, see Bromwich *et al.* (2001). This first-order match was obtained from eqs. (3) through (7) for $\Delta x = 20$ km, $\tau_S = 150$ kPa, $n = 3$, $m = 2$, $A = 231 \pm 10$ kPa $a^{1/3}$, $B = 2$ kPa $a^{1/2}$ $m^{-1/2}$, $a = 0.5$ m/a, values of c and length L_s of flowlines in Fig. 3 that fit the profiles of each ice stream, and using values of f_T that give the best fit to ice flowline elevations following Wilch and Hughes (2000), from $f_T = 1$ at the heads of ice streams to $f_T = 0$ at interior ice divides. The value of A was obtained from the EGIG traverse to the ice divide just north of Jakobshavn Isbrae (Budd, 1969, p. 178). The value of B is from Denton and Hughes (1981, p. 248). Bedrock topography was available through NSIDC: http: //www-nsidc.Colorado.edu/data/nsidc-0092.html (Bamber *et al.*, 2001), and plotted along twenty-odd flowlines selected for one-dimensional constructions of flowline profiles. These flowlines typically meet the submarine glacial troughs in Fig. 3. At the last glacial maximum (LGM), these flowlines would have continued along the submarine glacial troughs to the edge of the Greenland continental shelf.

Figure 4 shows ice elevation contours at 200 m intervals, using the same values of A, B, a, and f_T used to produce Fig. 3, but with isostatic rebound of the bed computed for $r = r_o[\exp(-t/t_o) - 1]$, $t = 300$ years, and a time constant of $t_o = 5000$ years in eq. (5).

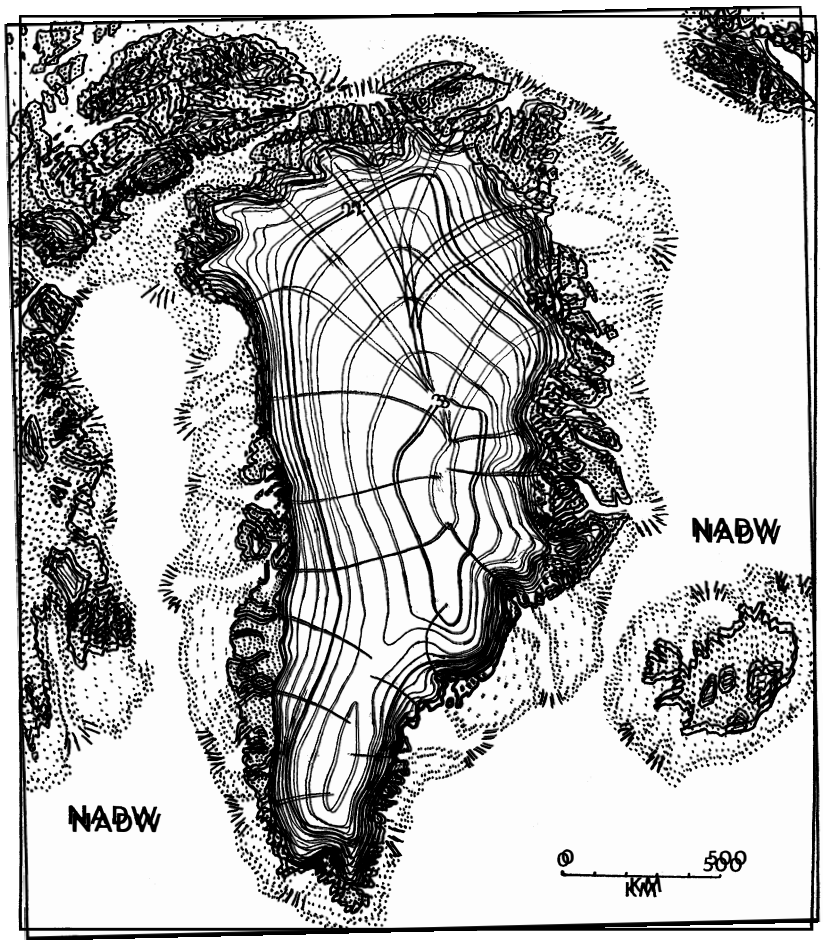

Fig. 3. The modeled present-day Greenland Ice Sheet. Heavily dotted areas are unglaciated lands above sea level. Lightly dotted areas are continental shelves below sea level. Undotted areas crossing continental shelves are troughs formerly occupied by marine ice streams. Short lines at seaward ends of troughs are glacial depositional fans deposited by the former ice streams at the last glacial maximum (LGM). North Atlantic Deep Water (NADW) is produced in the Labrador Sea and north of Iceland. Ice elevations for the Greenland Ice Sheet are shown at 0.2 km intervals, and were computed along flowlines from eq. (5) for $r=0$ such that pressure ratio P_W/P_I for stream flow in eq. (7) and basal thawed fraction f_T for sheet flow in eq. (6) give a best first-order fit to ice flowlines ending at the submarine glacial troughs, using average present-day surface accumulation and ablation rates and subglacial bed topography along these flowlines. The comparison with present-day 0.2 km contour intervals, see Bromwich et al. (2001), is as good as that obtained by Letréguilly et al. (1991). Clockwise from Jakobshavn Isbrae (J), best-fit values of c in eq. (7) for flowline lengths L_S are 100, 100, 100, 100, 85, 85, 80, 90, 80, 85, 85, 95, 95, 85, 55, 85, 80, 100, 100, 100, 100.

The values of c in eq. (7) were reduced from values in Fig. 3 to values in Fig. 4 for flowlines of length L_S in Fig. 4. In most cases these are the same lengths as in Fig. 3. High values of c in Fig. 3 for $t=0$ reflect the present-day short concave length of Greenland ice streams. The low values of c in Fig. 4 are comparable to those that fit present-day West Antarctic ice streams. Unchanged high values of c apply to flowlines where sheet flow extends to ice margins on land, notably in southwest Greenland, so that

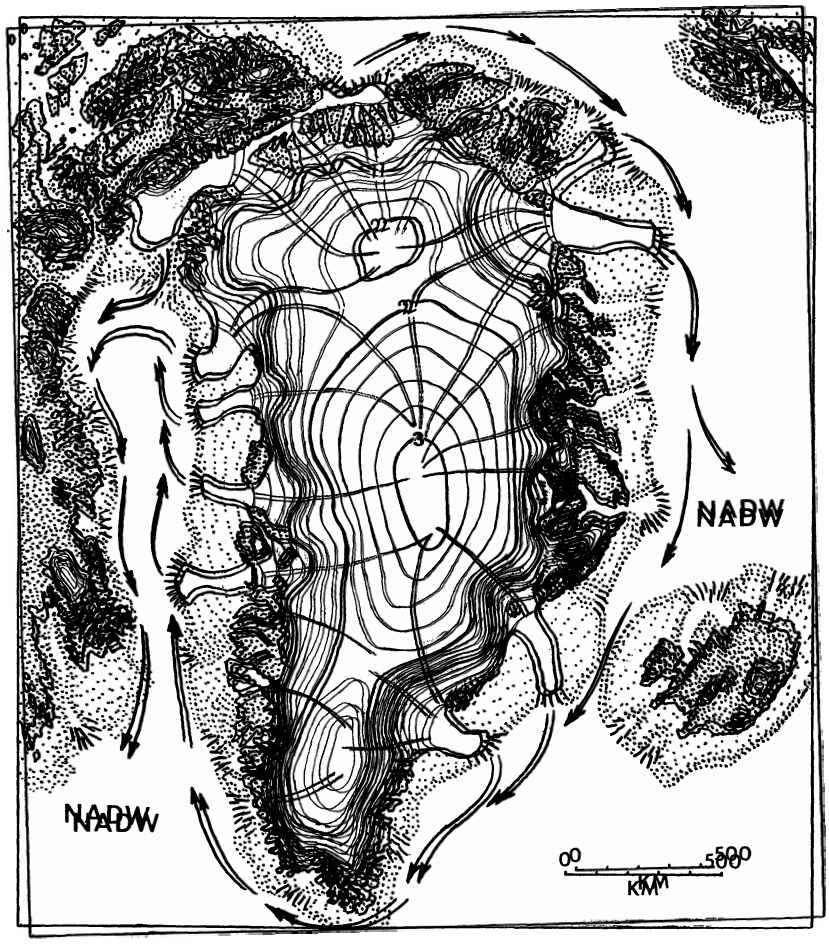

Fig. 4. The modeled Greenland Ice Sheet in 300 years. Ice elevations, plotted at 0.2 km intervals, were calculated from eq. (5) along flowlines similar to those used to produce Fig. 4, but with r calculated for $t=300$ a, values of P_W/P_I calculated from eq. (7) for values of c and L_S, and thawed faction f_T in eq. (6) that decreases in the same way as was done for Fig. 3, from unity at the heads of ice streams to zero at interior ice divides. Ice grounding lines are unchanged from those in Fig. 3. Arrows show the drift of icebergs calved from ice shelves floating in the submarine glacial troughs. Clockwise from Jakobshavn Isbrae (J), values of c in eq. (7) for flowline lengths L_S are obtained by making P_W/P_I proportional to surface ablation rates determined by Braithwaite and Olesen (1989), Braithwaite (1995), and Zwally and Giovinetto (2001), and are 25, 20, 30, 35, 20, 15, 10, 5, 90, 3, 10, 30, 80, 90, 90, 15, 25, 1, 2, 100, 100, 90.

$P_W/P_I \approx 0$. These high values of c produce flowline profiles similar to those produced by Huybrechts *et al*. (1991) and Huybrechts (1994, 1996) using their sheet-flow model.

Partial gravitational collapse of the Greenland Ice Sheet, shown in Fig. 4, results in a loss of 8×10^5 km^3 of ice. The resulting discharge of icebergs, 2.7×10^3 km^3/a, would be carried by ocean currents to sites of North Atlantic Deep Water (NADW) production, as shown by arrows in Fig. 4. Discharge of this ice volume in 300 years would shut down NADW production. Values of $\delta h_I/\delta t$ for use in eq. (5) are obtained by setting $\delta h_I/\delta t = 0$ and subtracting ice thicknesses after 300 years of thinning from the present-day thicknesses. When $\Delta h_I{}^*/\Delta x$ values are recalculated for these values of $\delta h_I/\delta t$, the new values are used to produce Fig. 4. A time of 600 years would not have changed the loss of ice volume significantly. This is seen by comparing $(1+r)^{1/2}$ in eq. (5), using $r = r_o\,[\exp(-t/t_o) - 1]$ when $t = 300$ a and $t = 600$ a for $r_o = 0.4$ and $t_o = 5000$ a. The northern Greenland ice dome shown in Fig. 4 was generated by excessive downdraw of ice due to high P_W/P_I (low c) values along ice flowlines that resulted in an ice saddle in the vicinity of the North GRIP drilling site (Kanagaratnanm *et al*., 2001). A high P_W/P_I value was found at this site when basal water rose far up the borehole.

4. Discussion and conclusions

This study employs a holistic approach that includes ice-streams as the vehicles for discharging icebergs. The ice surface lowering from Fig. 3 to Fig. 4 that discharged enough icebergs to halt NADW production for 300 years is a consequence of allowing summer meltwater in the present-day ablation zone to reach the bed by way of crevasses and moulins. Rates of surface melting used for this purpose are those reported by Braithwaite and Olesen (1989), Braithwaite (1995), and Zwally and Giovinetto (2001). These melting rates were made proportional to P_W/P_I by an appropriate selection of constant c in eq. (7). For the accumulation zone, $0 \leq P_W/P_I \ll 1$ and sheet flow were assumed, with $f_T = 0$ at ice divides and $f_T = 1$ at the heads of ice streams in eq. (6). Subglacial hydrology needs to be incorporated in a holistic thermo-mechanical model of ice flow, so that P_W/P_I variations along ice streams are based on physics, as outlined by eq. (3), not on empirical observations. This study points in that direction, but takes only one step. Can Greenland discharge enough icebergs in 300 years to shut down NADW production and trigger a rapid change in climate? The major conclusion of this study is that all available models are too simplistic to answer that question. The full complexity of the glaciological dimension to the question will now be discussed.

Ice-stream lengthening and lowering is missing from ice-sheet models by Huybrechts (1990, 1994, 1996) and Huybrechts *et al*. (1991) that were applied to Greenland, so that profile 1 only lowers to profile 2 in Fig. 2. The reason is because the longitudinal gravitational driving force in their models is determined only by the ice thickness and surface slope, so "greenhouse" warming only allows the ice margin to retreat and steepen, with little of the interior thinning shown by profile 3 in Fig. 2. Little or no thinning would be the behavior of ice ridges between ice streams, as Hindmarsh and LeMeur (2001) have shown. To take this into account, grounding lines were not allowed to retreat as ice thins in going from Fig. 3 to Fig. 4. This has the advantage of minimizing basal isostatic rebound at ice-stream grounding lines, because

ice thinning at grounding lines is minimized.

An important simplification in the present study is not allowing flowband widths to change in space and time. Bougamont *et al*. (2002, 2003) have shown that the concave profiles of West Antarctic ice streams can be produced if ice streams widen downstream, even in the absence of increased basal buoyancy downstream. This widening is prohibited for nearly all Greenland ice streams because they end as outlet glaciers that enter fjords having fixed widths. In the absence of downstream widening, and of increased basal buoyancy, a reduction of basal shear stress τ_O must be accompanied by an increase of side shear stress τ_S if ice streams are to maintain their high velocities. However, this produces the convex profiles of sheet flow, not the concave profiles of stream flow (Van der Veen, 1999, Figure 6.2). It is unfortunate that in the dozens of boreholes through concave West Antarctic ice streams drilled by Engelhardt and Kamb (1997), there were no strings of boreholes drilled along their central flowline to determine how P_W/P_I changes from the grounding line to the ice divide. The P_W/P_I variations would provide a way to assess c values used in eq. (7).

There is an obvious danger in not treating the full suite of positive and negative feedbacks in ice streams. For example, Van der Veen (2001) considered only removing ice-shelf buttressing to generate a positive feedback, that is countered by increased side shear as a negative feedback, for a Greenland ice stream. He concluded that no net thinning over time would occur, which is the opposite result from the different combinations of positive and negative feedbacks presented here. As another example, ice thinning increases vertical heat transport, which should eventually convert basal melting to basal freezing and thereby shut down an ice stream (Bougamont *et al*., 2002, 2003).

Thomas (2004) examined the effect of feedbacks in his holistic force-perturbation analysis of the present rapid thinning of Jakobshavn Isbrae that has accompanied disintegration of its floating terminus, and lubrication of its bed by meltwater in a surface lake that reaches the bed by way of crevasses. He found that the duration of thinning becomes longer as the ice drainage region expands, making ice flow faster and more convergent. This effect was not considered here and it would be minimized by the requirement that major ice streams undergo accelerated thinning nearly simultaneously. Thomas (2004) also found that the increase in $\dot{\varepsilon}_{xx}$ that causes accelerated downdraw of interior ice when the floating terminus disintegrates is eventually overcome by the reduced ice thickness, resulting in a new stable flowline profile, probably in much less than 300 years. He then shows how parts of the flowband might thickness and slow as other parts thin and speed up. These and other feedbacks examined by Thomas (2004) point to extreme caution in making generalizations about future behavior of the Greenland Ice Sheet, based on the present behavior of one or even of several ice streams. The Appendix compares the Thomas (2004) holistic approach to the one used here.

In view of these considerations, it is probably unfortunate that thinning of Greenland ice in 300 years calculated here just happens to produce an iceberg flux that could halt NADW production and trigger global cooling. Not only is an adequate understanding lacking for the dynamics of the Greenland Ice Sheet, it is also lacking for the surrounding ocean and atmosphere, especially in response to such a large discharge of ice. For example the area of NADW production, $10^6\,\mathrm{km}^2$, is not known with con-

fidence. Changing that area by a factor of two eliminates the coincidental match. Also simplifications in the model allow nearly the same ice thinning to be calculated for half or double the 300 years. Perhaps the iceberg outbursts from Greenland ice streams would not halt NADW production, but merely push the production sites farther south. Then atmospheric circulation might become more intense by increasing the equator-to-pole temperature gradient in the North Atlantic. This southward shift of the polar front might cause the warm North Atlantic Current to cross the ocean much further south, perhaps from Maine to Spain, as it did during the LGM. Any one of these alternatives is a possible worst-case scenario. The best-case scenario provides that feedbacks inherent in ice-sheet dynamics do not permit the kind of runaway ice thinning presented here. None of the models available now can predict a reliable scenario.

Acknowledgments

I thank referees Robert Thomas and Ralf Greve for suggesting substantial improvements and I thank B.A. Hughes for her patience in producing numerous drafts in reporting this study.

References

Andrews, J.T. (1970): A geomorphological study of post-glacial uplift with particular reference to Arctic Canada. London, Institute of British Geographers, 156.

Bamber, J.L., Layberry, R.L. and Gogineni, S. (2001): A new ice thickness and bed data set for the Greenland ice sheet 1. Measurement, data reduction, and errors. J. Geophys. Res., **106** (D24), 33773–33780.

Bougamont, M., Tulaczyk, S. and Joughin, I.R. (2002): Response of subglacial sediments to basal freeze-on: II. Application in numerical modeling of the recent stoppage of Ice Stream C, West Antarctica. J. Geophys. Res., **107** (B4).

Bougamont, M., Tulaczyk, S. and Joughin, I.R. (2003): Numerical investigations of the slowdown of Whillans Ice Stream, West Antarctica: is it Shutting Down like Ice Stream C? Ann. Glaciol., **37**, 239–246.

Braithwaite, R.J. (1995): Positive degree-day factors for ablation on the Greenland Ice Sheet studies by energy-balance modeling. J. Glaciol., **41**, 153–160.

Braithwaite, R.J. and Olesen, O.B. (1989): Calculation of glacier ablation from air temperature, West Greenland. Glacier Fluctuations and Climate Change, ed. by J. Oerlemans. Dordrecht, Kluwer, 219–233.

Broecker, W.S. and Denton, G.H. (1989): The role of ocean-atmosphere reorganizations in glacial cycles. Geochim. Cosmochim. Acta, **53**, 2465–2501.

Bromwich, D.H., Chen, Q.-S., Bai, L.-S., Cassano, E.N. and Li, Y. (2001): Modeled precipitation variability over the Greenland ice sheet. J. Geophys. Res., **106** (D24), 33891–33908.

Budd, W.F. (1969): The Dynamics of Ice Masses. Antarctic Division, Department of Supply.

Budd, W.F., Keage, P.L. and Blundy, N.A. (1979): Empirical studies of ice sliding. J. Glaciol., **23**, 157–170.

Denton, G.H. and Hughes, T.J., ed. (1981): The Last Great Ice Sheets. New York, Wiley, 437–467.

Engelhardt, H. and Kamb, B. (1997): Basal hydraulic system of a West Antarctic ice stream: constraints from borehole observations. J. Glaciol., **43**, 207–230.

Erngaard, E. (1972): Greenland-Then and Now. Copenhagen, Lademann, 240 p.

Glen, J.W. (1958): The flow law of ice. Symposium de Chamonix 16–24 Sept. 1958: Physique du Mouvement de la Glace. Gentbrugge, Association Internationale d'Hydrologie Scientifique, 171–183 (Publication No. 47).

Greve, R. (1997): Application of a polythermal three-dimensional ice sheet model to the Greenland Ice Sheet:

Response to steady-state and transient climate scenarios. J. Climate, **10**, 301–318.
Hindmarsh, R.C.A. and LeMeur, E. (2001): Dynamic processes involved in the retreat of marine ice sheets. J. Glaciol., **47**, 271–282.
Hughes, T. (1992): On the pulling power of ice streams. J. Glaciol., **38**, 125–151.
Hughes, T. (1998): Ice Sheets. New York, Oxford University Press, 343 p.
Hughes, T.J. (2003): The geometrical force balance in glaciology. J. Geophys. Res., **108** (B11), 2526–2543.
Hutter, K. (1983): Theoretical Glaciology: Material Science of Ice and the Mechanics of Glacier and Ice Sheets. Rotterdam, D. Reidel. 510 p.
Huybrechts, P. (1990): A 3-D model for the Antarctic Ice Sheet: a sensitivity study on the glacial-interglacial contrast. Climate Dyn., **5** (2), 79–92.
Huybrechts, P. (1994): The present evolution of the Greenland Ice Sheet: an assessment by modelling. Global Planet. Change, **9**, 39–51.
Huybrechts, P. (1996): Basal temperature conditions of the Greenland ice sheet during the glacial cycles. Ann. Glaciol., **23**, 226–236.
Huybrechts, P., Letreguilly, A. and Reeh, N. (1991): The Greenland ice sheet and greenhouse warming. Global Planet. Change, **3**, 399–412.
Joughin, I., Kwok, R. and Fahnestock, M.A. (1996a): Estimation of ice-sheet motion using satellite radar interferometry: method and error analysis with application to Humboldt Glacier, Greenland. J. Glaciol., **42**, 564–575.
Joughin, I., Tulaczyk, S., Fahnestock, M.A. and Kwok, R. (1996b): A mini-surge on the Ryder Glacier, Greenland, observed by satellite radar. Science, **274**, 228–230.
Kanagaratnam, P., Gogineni, S.P., Gundestrup, N. and Larsen, L. (2001): High-resolution radar mapping of internal layers at the North Greenland Ice Core Project. J. Geophys. Res., **106** (D24), 33799–33811.
Lange, M. and MacAyeal, D.R. (1986): Numerical models of the Filchner-Ronne Ice Shelf: An assessment of re-interpreted ice thickness distributions. J. Geophys. Res., **91**, 10457–10462.
Letréguilly, A., Huybrechts, P. and Reeh, N. (1991): Steady state characteristics of the Greenland ice sheet under different climates. J. Glaciol., **37**, 149–157.
MacAyeal, D.R. and Thomas, R.H. (1982): Numerical modeling of ice-shelf motion. Ann. Glaciol., **3**, 189–194.
Mayewski, P.A., Meeker, L.D., Twickler, M.S., Whitlow, S., Yang, Q. and Prentice, M. (1997): Major features and forcing of high latitude Northern Hemisphere atmospheric circulation over the last 110,000 years. J. Geophys. Res., (Special Issue-Oceans/Atmosphere): **102** (C12), 26345–26366.
Nyhoff, L. and Leestma, S. (1996): FORTRAN 77 for Engineers and Scientists. Upper Saddle River, NJ, Prentice Hall. 4th ed. 884 p.
Nye, J.F. (1952): The mechanics of glacier flow. J. Glaciol., **2**, 82–93.
Orowan, E. (1949): Remarks at a joint meeting of the British Glaciological Society. The British Rheologists Club, and the Institute of Metals. J. Glaciol., **1**, 231–236.
Raymond, C.F., Echelmeyer, K.A., Whillans, I.M. and Doake, C.S.M. (2001): Ice Stream Shear Margins. The West Antarctic Ice Sheet: Behavior and Environment, ed. by R.B. Alley and R.A. Bindschadler. Washington, D.C., American Geophysical Union, 137–156 (Antarctic Research Series, **77**).
Rignot, E.J., Gogineni, S.P., Krabill, W.B. and Ekholm, S. (1997): North and Northeast Greenland ice discharge from satellite radar in interferometry. Science, **276**, 934–937.
Schnitker, D. (1979): The deep waters of the western North Atlantic during the past 24,000 years, and the reinitiation of the Westerly Boundary Undercurrent. Mar. Micropaleontol., **4**, 265–280.
Thomas, R.H. (1973a): The creep of ice shelves: theory. J. Glaciol., **12**, 45–53.
Thomas, R.H. (1973b): The creep of ice shelves: interpretation of observed behaviour. J. Glaciol., **12**, 55–70.
Thomas, R.H. (2004): Force-perturbation analysis of recent thinning and acceleration of Jakobshavn Isbrae, Greenland. J. Glaciol., **50** (in press).
Thomas, R.H., Abdalati, W., Akins, T.L., Csatho, B.M., Frederick, E.B., Gogineni, S.P., Krabill, W.B., Manizade, S.S. and Rignot, E.J. (2000): Substantial thinning of a major east Greenland outlet glacier. Geophys. Res. Lett., **27**, 1291–1294.
Thomas, R.H., Abdalati, W., Frederick, E.B., Krabill, W.B., Manizade, S. and Steffen, K. (2003): Investigation of surface melting and dynamic thinning of Jakboshavns Isbrae, Greenland. J. Glaciol., **49**, 231–

239.
Tulaczyk, S.M., Kamb, B. and Engelhardt, H.F. (2001a): Estimates of effective stress beneath a modern West Antarctic ice stream from till preconsolidation and void ratio. Boreas, **30**, 101–114.
Tulaczyk, S.M., Scherer, R.P. and Clark, C.D. (2001b): A ploughing model for the origin of weak tills beneath ice streams: a qualitative treatment. Quat. Int., **86**, 59–70.
Van der Veen, C.J. (1983): A note on the equilibrium profile of a free floating ice shelf. The Netherlands, Institut voor Meteorologie en Oceanografie, Rijksuniversiteit-Utrecht, **83**–**15**, 15.
Van der Veen, C.J. (1999): Fundamentals of Glacier Dynamics. Rotterdam, A.A. Balkema, 462 p.
Van der Veen, C.J. (2001): Greenland ice sheet response to external forcing. J. Geophys. Res., **106** (D24), 34047–34058.
Weertman, J. (1957a): Deformation of floating ice shelves. J. Glaciol., **3**, 38–42.
Weertman, J. (1957b): On the sliding of glaciers. J. Glaciol., **3**, 33–38.
Weis, M., Greve, R. and Hutter, K. (1999): Theory of shallow ice shelves. Contin. Mech. Thermodyn., **11**, 15–50.
Wilch, E. and Hughes, T. (2000): Mapping basal thermal zones beneath the Antarctic ice sheet. J. Glaciol., **46**, 297–310.
Zotikov, I.A. (1986): The Thermophysics of Glaciers. Dordrecht, D. Reidel, 275 p.
Zwally, H.J. and Giovinetto, M.B. (2001): Balance mass flux and ice velocity across the equilibrium line in drainage systems of Greenland. J. Geophys. Res., **106** (D24), 33717–33728.
Zwally, H.J., Abdalati, W., Herring, T., Larson, K., Saba, J. and Steffen, K. (2002): Surface Melt-Induced Acceleration of Greenland Ice-Sheet Flow. Science, **297**, 218–222.

Appendix

It is instructive to compare the holistic approach used here with the one by Thomas (2004). This holistic approach emerges from a geometrical force balance in which basal water pressure P_W is represented by an equivalent water height h_W such that $P_W = \rho_W g h_W$, where h_W is equivalent to ice height $h_W(\rho_W/\rho_I)$. Then the part of basal ice overburden pressure $P_I = \rho_I g h_I$ for ice thickness h_I that is supported by the bed, not by basal water, is $h_I - h_W(\rho_W/\rho_I)$. Basal resistance to ice motion over incremental basal area $w_I \Delta x$ increases ice elevation by Δh and introduces a basal drag force given by:

$$F_O = \tau_O w_I \Delta x = \rho_I g [h_I - h_W(\rho_W/\rho_I)] w_I \Delta h, \tag{A1}$$

where τ_O is the basal shear stress. Equation (A1) gives τ_O in eq. (4):

$$\tau_O = \rho_I g = [h_I - h_W(\rho_W/\rho_I)] \Delta h / \Delta x. \tag{A2}$$

Ice thickness $h_W(\rho_W/\rho_I)$ supported by basal water pressure P_W must satisfy the Weertman (1957a) solution for longitudinal tensile force F_T in floating ice. He found tensile stress σ_T by subtracting the gravitational back force caused by average water pressure $\bar{P}_W$ from the gravitational forward force caused by average ice pressure $\bar{P}_I$ when $P_W/P_I = 1$. Allowing partial grounding, $P_W/P_I = \rho_W h_W/\rho_I h_I$ and:

$$\begin{aligned} F_T = \sigma_T w_I h_I &= [1/2 \rho_I g h_W(\rho_W/\rho_I)][w_I h_W(\rho_W/\rho_I)] - [1/2 \rho_I g h_W][w_I h_W] \\ &= [1/2 \rho_I g h_I (1 - \rho_I/\rho_W)(P_W/P_I)^2] w_I h_I, \end{aligned} \tag{A3}$$

where $P_W/P_I < 1$ when $h_I > h_W(\rho_W/\rho_I)$. Solving eq. (A3) for σ_T:

$$\sigma_T = 1/2 \rho_I g h_I (1 - \rho_I/\rho_W)(P_W/P_I)^2. \tag{A4}$$

Using the flow law of ice (Glen, 1958), the longitudinal strain rate $\dot{\varepsilon}_{xx}$ caused by longitudinal deviator stress σ'_{xx} and used in this study is given by (Hughes, 1998, p. 53–55):

$$\dot{\varepsilon}_{xx}=\left[\frac{1}{2}+\frac{1}{2}\left(\frac{\dot{\varepsilon}_{yy}}{\dot{\varepsilon}_{xx}}\right)^2+\frac{1}{2}\left(\frac{\dot{\varepsilon}_{zz}}{\dot{\varepsilon}_{xx}}\right)^2+\left(\frac{\dot{\varepsilon}_{xy}}{\dot{\varepsilon}_{xx}}\right)^2+\left(\frac{\dot{\varepsilon}_{yz}}{\dot{\varepsilon}_{xx}}\right)^2+\left(\frac{\dot{\varepsilon}_{zx}}{\dot{\varepsilon}_{xx}}\right)^2\right]^{\frac{n-1}{2}}\left(\frac{\sigma'_{xx}}{A}\right)^n$$

$$=R\left[\frac{\sigma_T}{(2+\dot{\varepsilon}_{yy}/\dot{\varepsilon}_{xx})A}\right]^n=\frac{R}{(2+\dot{\varepsilon}_{yy}/\dot{\varepsilon}_{xx})^n}\left[\frac{\rho_I g h_I}{2A}\left(1-\frac{\rho_I}{\rho_W}\right)\left(\frac{P_W}{P_I}\right)^2\right]^n, \qquad \text{(A5)}$$

where $\sigma_T=(2+\dot{\varepsilon}_{yy}/\dot{\varepsilon}_{xx})\sigma'_{xx}$ strain rates $\dot{\varepsilon}_{xy}=\dot{\varepsilon}_{yy}=\dot{\varepsilon}_{zy}=\dot{\varepsilon}_{zx}=0$ is assumed for the centerline of ice streams, so $\dot{\varepsilon}_{xx}=-\dot{\varepsilon}_{zz}$ and $R=1$, A is a temperature dependent ice hardness parameter, and $n\approx 3$ is an ice viscoplastic parameter.

Equation (A5) can be compared with the force perturbation model developed by Thomas (2004), who applied it to study newly accelerated thinning of Jakobshavns Isbrae in Greenland. In his force perturbation model:

$$\dot{\varepsilon}_{xx}\approx k(ch_I-P)^n, \qquad \text{(A6)}$$

where $k=R/(2+\dot{\varepsilon}_{yy}/\dot{\varepsilon}_{xx})^n A^n$, $c=\rho_I g/2$, $n=3$, and P is the total back pressure acting at distance x from the ice-sheet margin, as measured along an ice flowline. Back pressure results from side shear and basal shear along x, from water pressure at an ice-shelf grounding line, and from any confinement of the ice shelf. Differentiating eq. (A6) with respect to time t yields the following relationship between small perturbations ΔP in back-pressure and the resulting changes $\Delta\dot{\varepsilon}_{xx}$ and Δh_I in longitudinal strain rate and ice thickness, respectively:

$$\Delta\dot{\varepsilon}_{xx}/\dot{\varepsilon}_{xx}\approx(\Delta k/k)+3(c\Delta h_I-\Delta P)/(cH_I-P)\approx(\Delta k/k)$$
$$+3(c\Delta h_I-\Delta P)(k/\dot{\varepsilon}_{xx})^{1/3}. \qquad \text{(A7)}$$

Equation (A5) conforms with eq. (A6) when $P_W/P_I=1$, for which $\rho_I h_I=\rho_W h_W$, so that when $x=0$ at an ice-shelf grounding line, then for $x>0$ up an ice flowband:

$$\dot{\varepsilon}_{xx}=\frac{R}{(2+\dot{\varepsilon}_{yy}/\dot{\varepsilon}_{xx})^n}\left[\frac{\rho_I g h_I}{2A}-\frac{\rho_W g h_W}{2A}\left(\frac{h_W}{h_I}\right)\right]^n$$
$$=\frac{R}{[(2+\dot{\varepsilon}_{yy}/\dot{\varepsilon}_{xx})A]^n}\left[\left(\frac{\rho_I g}{2}\right)h_I-\frac{(1/2\rho_W g h_W)_0(w_I h_W)_0}{w_I h_I}-\frac{2\bar{\tau}_S\bar{h}_I x}{w_I h_I}-\frac{\bar{\tau}_O\bar{w}_I x}{w_I h_I}-P_{IS}\right]^n$$
$$=k(ch_I-F_I/w_I h_I)^n=k(ch_I-P)^n. \qquad \text{(A8)}$$

Here back pressure $P=F_I/w_I h_I$ results from a longitudinal back force F_I acting on transverse cross-sectional area $w_I h_I$ of an ice flowband, average water pressure at the grounding line, where $x=0$, is $(\bar{P}_w)_O=(1/2\rho_W g h_W)_O$ and exerts hydrostatic force $(F_W)_O=(1/2\rho_W g w_I h_w^2)_O$, $\bar{\tau}_S$, $\bar{h}_I$, $\bar{\tau}_O$, and $\bar{w}_I$ are averaged over distance x upslope from the grounding line, and P_{IS} is the back-pressure from a confined ice shelf. For an ice shelf, $h_W/h_I=\rho_I/\rho_W$ is constant all along x, but $h_W/h_I<\rho_I/\rho_W$ when partial grounding occurs. This is why $P_W/P_I=\rho_W h_W/\rho_I h_I$ is introduced in eq. (1).

If basal water rising in a borehole is not high enough to float the ice, as is observed

for West Antarctic ice streams (Engelhardt and Kamb, 1997), basal buoyancy ratio P_W/P_I must be introduced to account for a degree of basal grounding that prevents ratio h_W/h_I at x from attaining $h_W/h_I=\rho_I/\rho_W$ at grounding-line location $x=0$. A basal water pressure of P_W at $x>0$ is equivalent to a water load on the bed from water of height h_W above the bed, which is the same load as ice of height $h_W(\rho_W/\rho_I)=h_I(P_W/P_I)$ above the bed, compared to total ice height h_I. This equivalent water height produces a back force F_W of water at x given by:

$$F_W=(1/2\rho_W g h_W)(w_I h_W)=[1/2\rho_I g h_W(\rho_W/\rho_I)][w_I h_W]$$
$$=[1/2\rho_I g h_I(\rho_I/\rho_W)(P_W/P_I)^2][w_I h_I]. \quad \text{(A9)}$$

The remaining ice height, $h_I-h_W(\rho_W/\rho_I)=h_I(1-P_W/P_I)$, is supported by the bed and therefore is the ice height that drives the basal sliding "law" given by eq. (4). This is the main difference between the Thomas (2004) holistic approach and the holistic approach used here. Equation (5) is numerically integrated from $x=0$ at the ice front, so side drag and basal drag forces that cause stresses τ_S and τ_O, respectively, are summed cumulatively upslope from $x=0$. The hydrostatic force exerted by water pressure at $x=0$, and its upslope gradient, are included in the terms containing P_W/P_I and $\Delta(P_W/P_I)/\Delta_x$, respectively. Basal drag causes P_W/P_I to vary along x because it prevents perfect subglacial hydraulic conductivity. Side drag causes P_W/P_I to vary along x because it allows lost basal drag due to P_W/P_I under an ice stream to be partly transmitted across lateral shear zones to the bed between ice streams. All of these effects are numerically integrated along x, making eq. (5) holistic.